Impact of Surface Polyethylene Glycol (PEG) Density on Biodegradable Nanoparticle Transport in Mucus *ex Vivo* and Distribution *in Vivo*

Qingguo Xu,[†,‡] Laura M. Ensign,[†,‡,§] Nicholas J. Boylan,[‡,§] Arne Schön,[▽] Xiaoqun Gong,[†,‡,⊥,∥] Jeh-Chang Yang,[§] Nicholas W. Lamb,[†,‡] Shutian Cai,[§] Tao Yu,[⊗,‡] Ernesto Freire,[▽] and Justin Hanes[*,†,‡,§,⊗,#]

[†]Department of Ophthalmology, The Wilmer Eye Institute, The Johns Hopkins University School of Medicine, Baltimore, Maryland 21231, United States, [‡]Center for Nanomedicine, The Johns Hopkins University School of Medicine, Baltimore, Maryland 21231, United States, [§]Department of Chemical and Biomolecular Engineering, The Johns Hopkins University, Baltimore, Maryland 21218, United States, [⊥]Institute of Nanobiotechnology, School of Materials Science and Engineering, Tianjin University, Tianjin 300072, P.R. China, [∥]School of Life Science, Tianjin University, Tianjin 300072, P.R. China, [▽]Department of Biology, The Johns Hopkins University, Baltimore, Maryland 21218, United States, [⊗]Department of Biomedical Engineering, The Johns Hopkins University, Baltimore, Maryland 21205, United States, and [#]Departments of Environmental Health Sciences, Oncology, Neurosurgery, and Pharmacology & Molecular Sciences, The Johns Hopkins University, Baltimore, Maryland 21231, United States

ABSTRACT Achieving sustained drug delivery to mucosal surfaces is a major challenge due to the presence of the protective mucus layer that serves to trap and rapidly remove foreign particulates. Nanoparticles engineered to rapidly penetrate mucosal barriers (mucus-penetrating particles, "MPP") have shown promise for improving drug distribution, retention and efficacy at mucosal surfaces. MPP are densely coated with polyethylene glycol (PEG), which shields the nanoparticle core from adhesive interactions with mucus. However, the PEG density required to impart the "stealth" properties to nanoparticles in mucus, and thus, uniform distribution *in vivo*, is still unknown. We prepared biodegradable poly(lactic-*co*-glycolic acid) (PLGA) nanoparticles with a range of PEG surface densities by blending various ratios of a diblock copolymer of PLGA and 5 kDa poly(ethylene glycol) (PLGA—PEG_{5k}) with PLGA. We then evaluated the impact of PEG surface density, measured using an ^{1}H NMR method, on mucin binding *in vitro*, nanoparticle transport in freshly obtained human cervicovaginal mucus (CVM) *ex vivo*, and nanoparticle distribution in the mouse cervicovaginal tract *in vivo*. We found that at least 5% PEG was required to effectively shield the nanoparticle core from interacting with mucus components *in vitro* and *ex vivo*, thus leading to enhanced nanoparticle distribution throughout the mouse vagina *in vivo*. We then demonstrated that biodegradable MPP could be formulated from blends of PLGA and PLGA—PEG polymers of various molecular weights, and that these MPP provide tunable drug loading and drug release rates and durations. Overall, we describe a methodology for rationally designing biodegradable, drug-loaded MPP for more uniform delivery to the vagina.

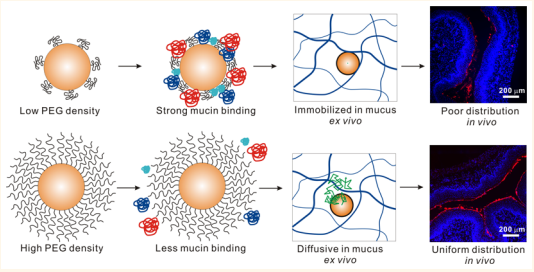

KEYWORDS: drug delivery · vagina · paclitaxel · PLGA · mucosal surface

Mucosal surfaces are often targeted for locally treating the many diseases that affect the mucosa, since systemic drug therapies are often ineffective or associated with systemic side effects.[1−3] Localized drug delivery to mucosal surfaces has many advantages over systemic administration, such as reduced systemic side effects and sustained drug levels at target sites.[4,5] However, mucus layers lining mucosal surfaces effectively trap pathogens, toxins, environmental fine particles, and conventional nanoparticle (CP) drug delivery systems *via* steric and/or adhesive interactions,[3,6] thereby preventing them from distributing uniformly. Natural mucus clearance mechanisms also facilitate the rapid removal of these trapped materials.[6] Therefore, mucus serves as a protective barrier that reduces the efficacy of localized drug and gene delivery at mucosal surfaces.[3,7]

Previously, we demonstrated that densely coating the surface of nanoparticles with low molecular weight polyethylene glycol (PEG) led to rapid diffusion of the nanoparticles through human mucus.[8,9] Furthermore,

* Address correspondence to hanes@jhmi.edu.

Received for review June 24, 2015 and accepted August 22, 2015.

Published online August 24, 2015
10.1021/acsnano.5b03876

administration of these mucus-penetrating particles (MPP) in a hypotonic vehicle induced fluid absorption by the epithelium that uniformly coated MPP over the tissue surface, providing prolonged retention and enhanced therapeutic efficacy in the mouse vagina.[10] In contrast, uncoated CP adhered to mucus and aggregated in the lumen.[10] Similar to CP, nanoparticles without a sufficiently dense PEG coating to shield the nanoparticle core from interactions with mucus should remain mucoadhesive, limiting their distribution and retention at mucosal surfaces. Therefore, we hypothesized that there is a minimum PEG density on the surface of nanoparticles that must be achieved for efficient penetration of mucus. Here, we evaluated the impact of PEG surface density on interactions between nanoparticles and mucus by formulating biodegradable nanoparticles composed of blends of poly(lactic-*co*-glycolic acid) (PLGA) and block copolymers of PLGA and PEG (PLGA–PEG) to allow for tunable PEG surface density. We then characterized the stability and binding of mucins to the surfaces of nanoparticles with various PEG densities *in vitro*, the transport of nanoparticles in freshly obtained human cervicovaginal mucus (CVM) *ex vivo*, and the distribution of the nanoparticles in the mouse cervicovaginal tract *in vivo*. We anticipate that the methodology described here will provide a framework for rationally designing biodegradable MPP for improved drug delivery to mucosal surfaces.

RESULTS AND DISCUSSION

Preparation of PLGA–PEG Nanoparticles. Biodegradable PLGA–PEG nanoparticles with varying target PEG contents (0, 2, 3, 5, 8, 10, and 25 wt %, referred to as PLGA, PLGA–$PEG_{2\%}$, PLGA–$PEG_{3\%}$, PLGA–$PEG_{5\%}$, PLGA–$PEG_{8\%}$, PLGA–$PEG_{10\%}$, and PLGA–$PEG_{25\%}$) were prepared using an emulsification method we previously described.[11] PEG with molecular weight of 5 kDa was used throughout our studies, as PLGA–PEG nanoparticles (PEG content of 6 wt %) with PEG molecular weights ranging from 1 to 10 kDa rapidly diffused in human cervicovaginal mucus (CVM).[11] The target PEG content was controlled by varying the ratio of PLGA to PLGA–PEG used in nanoparticle preparation. Nanoparticle diameters were controlled to around 100 nm by adjusting polymer concentration and emulsification parameters. All nanoparticle formulations were monodisperse (polydispersity index < 0.15) as determined by dynamic light scattering (Table 1). Nanoparticles exhibited spherical morphologies as observed by TEM (Figure 1).

Quantification of PEG Density. Coating nanoparticles with PEG to shield the surface can improve nanoparticle stability,[12] prolong blood circulation half-life,[13–16] and reduce interactions with biological tissues and fluids, including mucus.[8,17] Thus, various methods have been described for characterizing the extent of surface shielding provided by PEG on the surface of

TABLE 1. Physiochemical Characterization and Calculated PEG Surface Density

target PEG content (wt %)	D (nm)[a]	PDI	ζ-potential (mV)	total PEG content (wt %)	surface PEG content (wt %)	[Γ] (chains/100 nm^2)[b]	[Γ]/[Γ*][c]	D_w/D_m[d]
25	91 ± 5	0.094	−2.7 ± 0.7	13.7 ± 0.3	12.9 ± 1.0	30 ± 3	6.7 ± 0.7	6
10	117 ± 7	0.097	−2.4 ± 0.6	7.4 ± 0.1	7.2 ± 0.2	19 ± 1	4.4 ± 0.3	9
8	116 ± 8	0.068	−4.3 ± 0.9	6.0 ± 0.3	6.0 ± 0.3	16 ± 2	3.7 ± 0.4	8
5	106 ± 6	0.085	−7.0 ± 0.7	3.7 ± 0.1	3.7 ± 0.2	10 ± 0.2	2.4 ± 0.0	17
3	101 ± 6	0.078	−10 ± 0.1	2.5 ± 0.1	2.6 ± 0.1	6.5 ± 0.2	1.5 ± 0.1	142
2	91 ± 6	0.075	−20 ± 1.4	1.4 ± 0.4	1.4 ± 0.0	3.3 ± 0.1	0.8 ± 0.0	4,000
0	144 ± 6	0.056	−72 ± 2.2	N/A	N/A	N/A	N/A	38,000

[a] D is the diameter of nanoparticles. [b] The PEG density [Γ] is the number of PEG molecules (chains) on the nanoparticle surface per 100 nm^2 of surface area. [c] [Γ*] represents the number of unconstrained (mushroom conformation) PEG molecules that would occupy a surface area of 100 nm^2 on the nanoparticle surface. The ratio [Γ]/[Γ*] reflects how densely packed and, thus, constrained, the PEG molecules are on the nanoparticle surface. [d] Ratios of the ensemble average diffusion coefficients in water (D_w) compared to in CVM (D_m) at a time scale of 1 s.

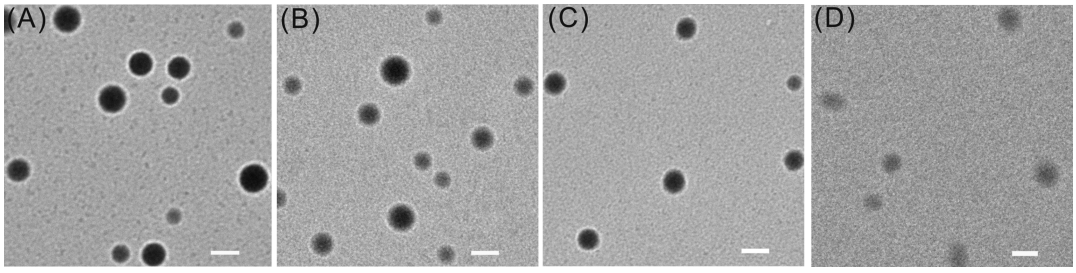

Figure 1. Representative TEM images for nanoparticles with various PEG contents: (a) 0%, (b) 3%, (c) 10%, and (d) 25% PEG. White scale bars = 100 nm.

nanoparticles. Here, we found that increasing the target PEG content resulted in increasingly near-neutral ζ-potential (surface charge), and near-neutral surface charge of approximately -2 to -7 mV was achieved with target PEG content of 5 wt % and higher (Table 1). However, we recently observed that near-neutral ζ-potential for PEG-coated polystyrene nanoparticles was necessary, but not sufficient, for nanoparticle penetration through the brain extracellular matrix, necessitating the development of a more sensitive assay for PEG surface density.[18] We describe here ^{1}H NMR methods for determining both the total PEG content and the surface PEG content, which provides additional information about the amount of incorporated PEG that successfully phase separates to the particle surface during particle formation. The surface PEG has a broadening peak around 3.65 ppm (Figure S1A,B), which can be used for quantitative analysis of PEG surface density.[11,19] As shown in Table 1, the surface PEG content on nanoparticles increased as the target PEG content increased. Next, the surface PEG density ([Γ], the number of PEG chains per 100 nm^2 assuming perfect spheres with smooth surfaces) was calculated and compared with the theoretical value required for full surface PEG coverage where PEG remains in the mushroom configuration regime ([Γ^*], the number of unconstrained PEG molecules per 100 nm^2).[11] PLGA–PEG$_{3\%}$ nanoparticles had a calculated surface PEG density of 6.5 PEG/100 nm^2 ([Γ]/[Γ^*] = 1.5), which indicated that the PEG was in the brush configuration. A dense brush conformation of PEG ([Γ]/[Γ^*] > 2) was achieved for PLGA–PEG nanoparticles with $\geq$5 wt % target PEG content (Table 1). The total PEG content within the nanoparticles was determined by dissolving the lyophilized PLGA–PEG nanoparticles in $CDCl_3$ prior to performing ^{1}H NMR measurements (Figure S1C). The total PEG content was similar to the nanoparticle surface PEG content, as shown in Table 1. Thus, our emulsification method allowed almost all of the PEG in the PLGA–PEG nanoparticles to phase separate to the particle surface. Slow extraction of dichloromethane from the emulsion droplets into the surrounding water phase likely provided sufficient time for the hydrophilic PEG chains to diffuse and assemble at the surface of the nanoparticles.[11,19] Interestingly, PLGA–PEG$_{10\%}$ nanoparticles prepared by nanoprecipitation (a solvent diffusion method) contained 6.5 wt % total PEG content, and only 89% of PEG chains were detected at surface (5.8 wt % surface PEG content) (Table S2). Thus, the emulsification method allowed for more complete partitioning of the hydrophilic PEG segments to the surface of the nanoparticles in comparison to the nanoprecipitation method.

Nanoparticle Stability. The colloidal stability of nanoparticles in the presence of proteins can be probed by dynamic light scattering (DLS) studies through monitoring the change in nanoparticle size and nanoparticle

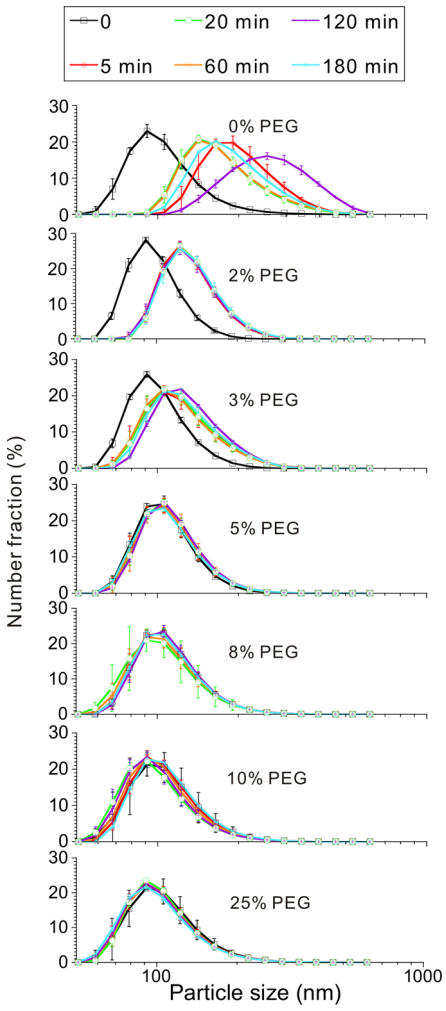

Figure 2. Size distribution of PLGA nanoparticles with various target PEG contents (0, 2, 3, 5, 8, 10, and 25% PEG) over time during incubation in 10 mg/mL mucin.

aggregation due to protein adsorption and biofouling.[20−22] Mucin can strongly bind to nanoparticles *via* various adhesive interactions, including hydrogen bonding and hydrophobic and electrostatic attractions.[3] By monitoring nanoparticle size in the presence of mucin using DLS, we studied how PEG surface density affects *in vitro* stability of nanoparticles. Nanoparticles were incubated with mucin solution (10 mg/mL) and particle size was monitored over time. As shown in Figure 2, in the absence of PEG (0% PEG), PLGA nanoparticles exhibited a dramatic size increase and broadening in particle size distribution over time in the mucin solution. The diameter of PLGA nanoparticles (0% PEG) increased from 109 $\pm$ 2 to 207 $\pm$ 9 nm within 5 min of incubation in mucin solution (Figure S3). A more minor increase in particle size (Figure S3) and lesser broadening in the nanoparticle size distribution (Figure 2) were observed for particles coated with PEG in a mushroom conformation (PLGA–PEG$_{2\%}$). PLGA–PEG$_{3\%}$ nanoparticles with surface density of 6.5 PEG/100 nm^2 and a brush-like PEG architecture ([Γ]/[Γ^*] > 1) still exhibited

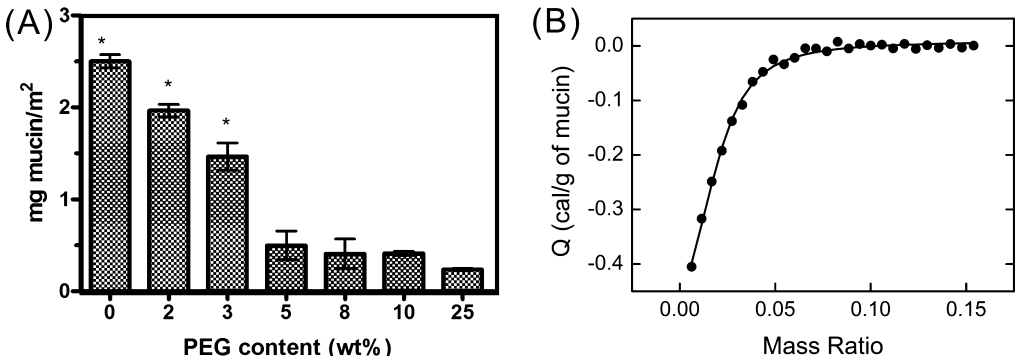

Figure 3. (A) Mucin binding to the surface of PLGA nanoparticles with various target PEG contents (0, 2, 3, 5, 8, 10, and 25% PEG). The amount of bound mucin is expressed as mg mucin/m^2 of nanoparticle surface area. (B) A representative image of the raw data collected from the isothermal titration calorimetry (ITC) experiment for mucin binding to PLGA−PEG$_{10\%}$ nanoparticles. Results represented as mean ± SD from 3 replicates.

broadening of particle size distribution (Figure 2) and a 30% increase in particle diameter (Figure S3) after incubation in mucin solution within 5 min. In contrast, PLGA−PEG nanoparticles with 5−25% PEG content ($[\Gamma]/[\Gamma^*] \geq 2$, indicating PEG in the dense brush conformation) were stable in mucin solution and retained their original hydrodynamic diameter during the entire 3 h incubation.

Mucin Binding *in Vitro*. Reduced mucin-binding *in vitro* has previously been shown to correlate with rapid penetration of nanoparticles through mucus.[8,23−25] Here, we quantified the amount of mucin that adsorbed to the nanoparticle surface with isothermal titration calorimetry (ITC). ITC has been successfully used to determine nanoparticle−protein interactions, and the stoichiometry of proteins bound per nanoparticle can be derived from the binding curves.[12,26] In good agreement with the results of the *in vitro* nanoparticle stability tests, Figure 3 shows that the amount of bound mucin per m^2 of nanoparticle surface area significantly decreased as PEG surface density increased. The amount of mucin that bound to the surface of PLGA−PEG nanoparticles decreased slightly as the PEG content increased from 0% to 3%. Similarly, the amount of mucin bound to the surface of PLGA−PEG nanoparticles reached a minimum plateau value (0.50 ± 0.16 mg mucin/m^2) when the PEG content was 5% or higher, corresponding to particles with surfaces coated with PEG in the dense brush conformation.

Various other methods have also been used to quantify the amount of protein bound to nanoparticles. The amount of bound protein can be indirectly measured after washing nanoparticles, though some of the bound protein is likely to be lost from the nanoparticle surface during washing.[20] Other methods, such as DLS[27] and fluorescence correlation spectroscopy (FCS),[21,28] can be used to quantify protein binding by measuring the hydrodynamic radii of nanoparticles in the presence of protein. To achieve meaningful quantification through DLS, nanoparticles should be colloidally stable, and nanoparticle size should be significantly larger (≥10 nm) than the protein to avoid the light scattering influence from free proteins, but nanoparticle size should be small (<100 nm) enough to show a feasible size increase after the protein binding (typically hydrodynamic radii ≤ 5 nm).[20] FCS can avoid the interference of free protein molecules by only measuring the fluorescent protein−NP complexes, but it requires the fluorescence labeling of nanoparticles and is only sensitive to smaller nanoparticles.[20,21]

Nanoparticle Transport in Human Mucus *ex Vivo*. We next used multiple particle tracking (MPT) to observe the transport dynamics of fluorescently labeled nanoparticles in freshly obtained, undiluted human CVM. PLGA nanoparticles without PEG (0% PEG) were completely immobilized in CVM (Figure 4A), with an average diffusivity that was 38 000 times slower than their theoretical diffusivity in water (D_w/D_m) (Table 1). Compared to PLGA nanoparticles, PLGA−PEG$_{2\%}$ (2% PEG) and PLGA−PEG$_{3\%}$ (3% PEG) nanoparticles exhibited increased diffusivity in mucus; the ratios of the ensemble average diffusion coefficients in water compared to those in CVM (D_w/D_m) were 4000 and 142, respectively, but the nanoparticle motions remained highly constrained (Figure 4A). Further increasing the PEG content to 5% produced nanoparticles that diffused only 17-fold slower in mucus than their theoretical diffusivity in water (Table 1). As shown in Figure 4B, the ensemble-averaged mean square displacements (⟨MSD⟩) of nanoparticles in CVM increased as PEG content increased from 0% to 5%, with only minor additional increases in ⟨MSD⟩ for nanoparticles with 8−25% PEG content. We characterized the heterogeneity in the transport of individual particles within the ensembles by plotting the distribution of the logarithms of individual particle effective diffusivities (D_{eff}) at τ = 1s (Figure 4C). Over 90% of the PLGA−PEG nanoparticles with dense brush PEG coatings (target PEG content ≥5 wt %) exhibited D_{eff} values greater than 0.1 μm^2/s. In contrast, only 64% of PLGA−PEG$_{3\%}$, 18% of PLGA−PEG$_{2\%}$, and 0% of PLGA nanoparticles diffused at the rapid speed of 0.1 μm^2/s or greater. In addition to

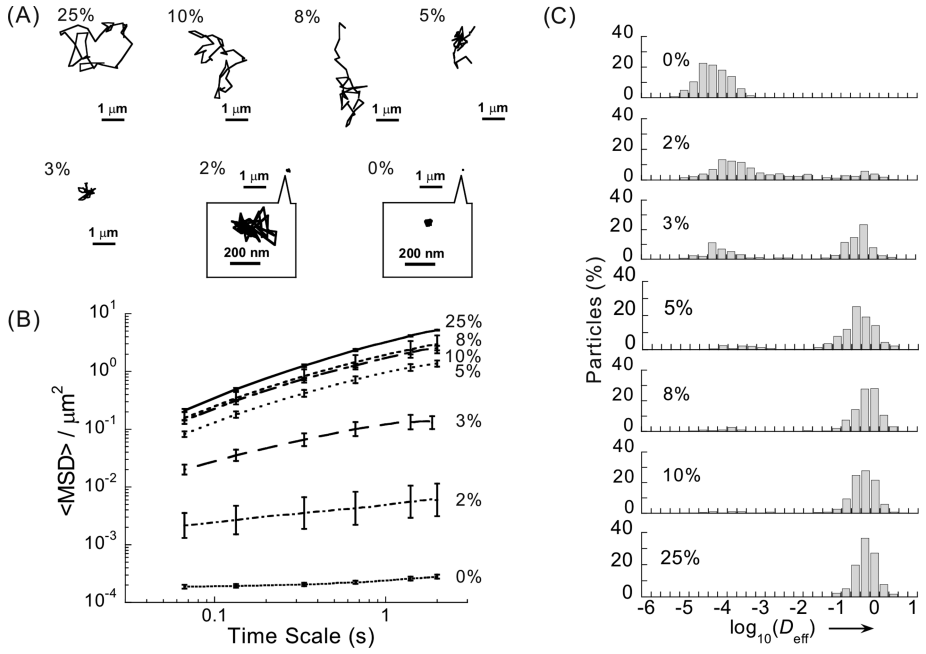

Figure 4. Transport of PLGA nanoparticles with various target PEG contents (0, 2, 3, 5, 8, 10, and 25% PEG) in fresh, undiluted CVM. (A) Representative trajectories for 3 s of particle motion. (B) Ensemble-averaged geometric mean square displacement (⟨MSD⟩) as a function of time scale. (C) Distributions of the logarithms of individual particle effective diffusivities (D_{eff}) at a time scale of 1 s. Data represent three independent experiments with ≥120 nanoparticles tracked for each experiment (mean ± SEM).

facilitating rapid penetration in mucus, dense PEG surface coatings may also be beneficial for shielding nanoparticles from serum protein adsorption and macrophage uptake.[12,29] It was found that between 2 and 5 wt % PEG content in poly(lactic acid)−PEG (PLA−PEG) nanoparticles was the threshold for optimal serum protein resistance.[29] The optimal plasma circulation lifetime of liposomes was reported to be achieved at 2 mol % 1,2-distearoyl-*sn*-glycero-3-phosphatidylethanolamine (DSPE) modified with PEG2000 (DSPE−PEG2000).[30]

Mucus is composed of mucin fibers secreted by goblet cells and submucosal glands. Mucins contain both globular regions with small exposed hydrophobic patches and densely glycosylated and negatively charged regions.[6] The hydrophobicity and negative charge on mucin fibers greatly contribute to the high viscoelasticity and stickiness of mucus.[6] When nanoparticle PEG surface density was low, the nanoparticle surface was not shielded from interactions with soluble mucins in the mucin binding assay, which correlated with immobilization within the mucus mesh in human CVM *ex vivo* (Figure 5). To most effectively minimize mucin binding, we found that a dense brush conformation ($[\Gamma]/[\Gamma^*] > 2$) was required, which was achieved for PLGA−PEG nanoparticles with ≥5% target PEG content. High PEG surface density minimized the adhesion of mucin fibers to PLGA−PEG nanoparticles *in vitro*, resulting in rapid diffusion in human CVM *ex vivo* (Figure 5).

Nanoparticle Distribution *in Vivo*. For effective vaginal drug delivery, uniform distribution deep into the folded vaginal epithelium (rugae) and over the entire

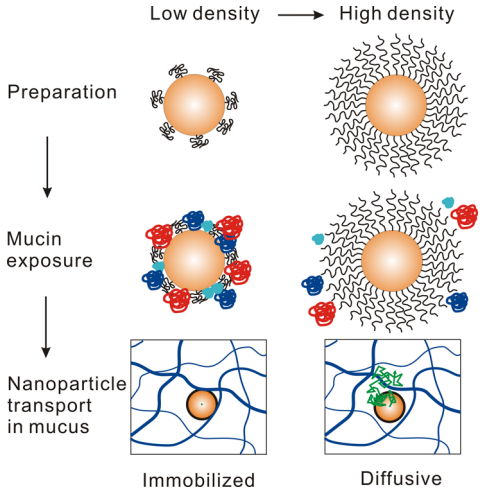

Figure 5. Schematic illustrating the effect of nanoparticle PEG surface density on transport behavior in mucus showing that nanoparticles with low density PEG coatings adhered to mucus (blue mesh) allowing the access of mucin molecules to nanoparticle core, whereas nanoparticles with high PEG surface density rapidly diffused through the open spaces in mucus *ex vivo* (particle trajectory depicted in green) by preventing the mucin adsorption. Low (light blue), intermediate (blue), and high molecular weight (red) mucin molecules are depicted in the middle row.

cervicovaginal mucosa is beneficial.[10,31−33] For example, poor drug distribution into the vaginal folds has been implicated as a cause for the failure of microbicides to protect against sexually transmitted infections.[34] Thus, we investigated how surface PEG density and *ex vivo* mucus penetration relates to nanoparticle distribution in the vagina of an estrus phase mouse

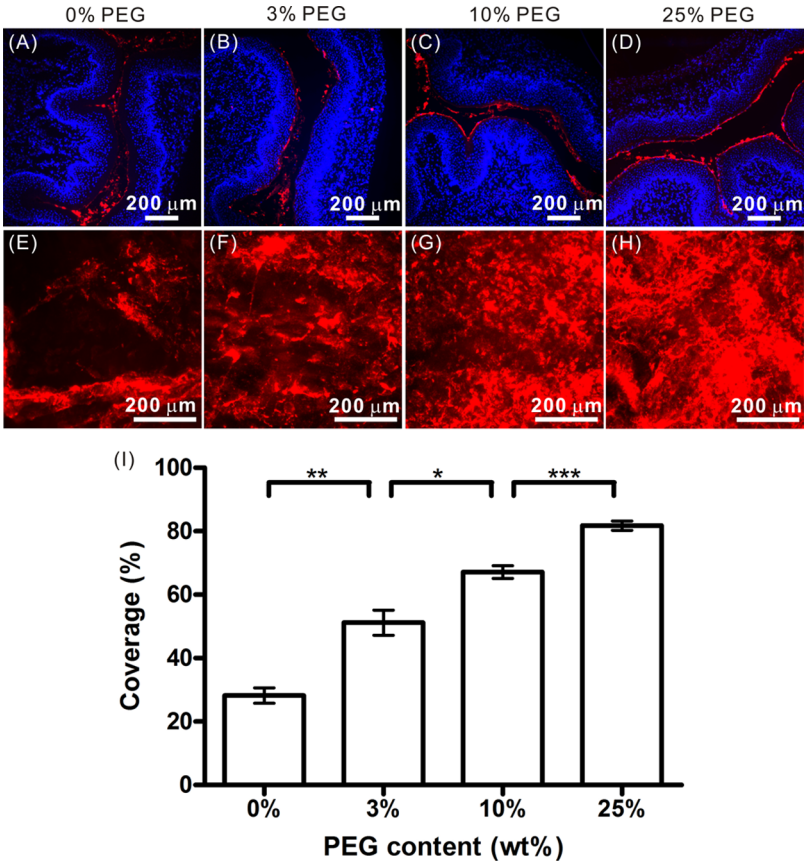

Figure 6. Distribution of nanoparticles in the mouse vagina *in vivo*. The distribution of red fluorescent (A and E) PLGA (0% PEG), (B and F) PLGA−$PEG_{3\%}$ (3% PEG), (C and G) PLGA−$PEG_{10\%}$ (10% PEG), and (D and H) PLGA−$PEG_{25\%}$ (25% PEG) in transverse cryosections of estrus phase mouse vaginal tissue (upper row) and on flattened estrus phase mouse vaginal tissue (bottom row). (I) The percent surface coverage by nanoparticles on the flattened vaginal tissue surface was quantified as percent coverage ± SEM.

model that more closely mimics the human vagina.[10] We administered fluorescently labeled PLGA−PEG nanoparticles with various PEG surface densities in a hypotonic vehicle (deionized water).[35] PLGA nanoparticles (no PEG coating) aggregated in the outer mucus layers and did not penetrate into the rugae (Figure 6A). PLGA−$PEG_{3\%}$ nanoparticles, found to have PEG surface density insufficient for uniform penetration in human CVM *ex vivo*, also aggregated in the outer mucus layers and provided a minor increase in vaginal tissue coverage compared to PLGA nanoparticles (Figure 6B). In contrast, both PLGA−$PEG_{10\%}$ and PLGA−$PEG_{25\%}$ nanoparticles, with highly dense PEG surface coatings, formed a continuous particle layer that coated the vaginal epithelium, including the surfaces of the rugae (Figure 6C,D). We then quantified the nanoparticle surface coverage on flattened vaginal tissue. Within 10 min of administration, vaginal tissues were excised, sliced open longitudinally, and flattened to expose the rugae. Similar to our previous report,[10] we observed "stripes" of mucoadhesive PLGA nanoparticles corresponding to contact with the luminal facing tissue surfaces, alternating with dark stripes corresponding to tissue contained within the rugae that did not come in contact with nanoparticles (Figure 6E). Nanoparticles with insufficient PEG surface coating (PLGA−$PEG_{3\%}$) demonstrated minimal improvement in vaginal surface coverage (Figure 6E) compared to PLGA nanoparticles. In contrast, densely PEG-coated nanoparticles (10 and 25% PEG) were drawn through mucus by water absorption to the epithelium, including penetration into the rugae, resulting in a uniform particle coating on the flattened vaginal surface (Figure 6G,H). We found that an increase in the target PEG content from 0% to 3% resulted in a significant increase in vaginal coverage ($p < 0.01$), from 28% to 51% of the tissue surface (Figure 6I). Further increases in the target PEG content to 10% and 25% led to increased vaginal surface coverage of 67% and 82%, respectively (Figure 6I). Although there was not a significant difference in the diffusion of PLGA−$PEG_{10\%}$ and PLGA−$PEG_{25\%}$ nanoparticles in human mucus *ex vivo*, the vaginal tissue surface coverage by PLGA−$PEG_{25\%}$ was significantly increased compared to the surface coverage by PLGA−$PEG_{10\%}$. The slightly larger diameter of the PLGA−$PEG_{10\%}$ nanoparticles (117 *versus* 91 nm for PLGA−$PEG_{25\%}$), may have led to reduced vaginal coverage. It is also possible that the minimum PEG surface density required for

TABLE 2. Characterization of Paclitaxel-Loaded Nanoparticles Prepared Using PLGA–PEG and Blends of PLGA/PLGA–PEG

PLGA	PLGA–PEG	*D* (nm)	PDI	ζ-potential (mV)	DL (%)[a]	EE (%)[b]	$T_{1/2}$ (days)[c]	[Γ] (chains/100 nm^2)	[Γ]/[Γ*]	D_w/D_m
$PLGA_{5.6k}$	$PLGA_{20k}$–PEG_{5k}	75 ± 4	0.08	−4.6 ± 1.7	6.9	76	2.5	18 ± 0.4	4.0 ± 0.1	6
$PLGA_{18k}$	$PLGA_{20k}$–PEG_{5k}	91 ± 2	0.10	−3.9 ± 0.4	5.6	62	5	17 ± 0.7	3.8 ± 0.2	5
$PLGA_{55k}$	$PLGA_{20k}$–PEG_{5k}	92 ± 8	0.13	−3.8 ± 0.9	5.5	60	6	17 ± 0.4	3.8 ± 0.1	5
-	$PLGA_{45k}$–PEG_{5k}	110 ± 4	0.08	−2.7 ± 0.4	2.2	24	1.5	20 ± 0.3	4.4 ± 0.1	7

[a] DL is the drug loading. [b] EE is the encapsulation efficiency. [c] $T_{1/2}$ represents the time to release 50% of encapsulated drug *in vitro*.

uniform penetration in mouse vaginal mucus may be higher than the minimum PEG surface density required for uniform penetration through *ex vivo* human mucus; we previously observed that a higher PEG surface density was required for nanoparticle penetration through brain tissue compared nanoparticle penetration through human CVM.[18] Nevertheless, this finding has a clear implication toward the design of biodegradable nanoparticles for delivery to mucosal surfaces: sufficient PEG surface density must be achieved for nanoparticles to rapidly diffuse through mucus, which leads to enhanced nanoparticle distribution at mucosal surfaces.

Drug Loading and Drug Release. Paclitaxel (PTX) is a model anticancer drug, which was demonstrated to be more efficacious for local treatment in a mouse model of highly aggressive cervical cancer when encapsulated within MPP compared to CP.[36] Thus, we formulated PTX-loaded PLGA–PEG nanoparticles using various molecular weight PLGA and PEG copolymers to provide tunable drug loading and drug release rates. As shown in Table 2 and Figure S4, we successfully produced several PTX-loaded nanoparticle formulations with high density PEG surface coatings, resulting in rapid nanoparticle penetration in human CVM. We prepared nanoparticles with 10% target PEG content composed of $PLGA_{45k}$–PEG_{5k} block copolymer or a blend of PLGA (MW 5.6, 18, and 55 kDa) with $PLGA_{20k}$–PEG_{5k} block copolymer. The blended nanoparticles were smaller in diameter than the $PLGA_{45k}$–PEG_{5k} nanoparticles, likely due to the increased hydrophobicity of the core from the blended PLGA (Table 2). The molecular weight and its distribution of PLGA did not affect the PEG surface density and the resulted mucus penetration properties of the blended nanoparticles. The calculated PEG surface density for all of the drug-loaded formulations was similar (Table 2) and above the threshold calculated for the PLGA–$PEG_{5\%}$ nanoparticles. As expected based on PEG surface density, all of the drug-loaded PLGA–PEG formulations displayed diffusive trajectories in CVM *ex vivo* (Figure S4A), high ⟨MSD⟩ across all time scales up to 3 s (Figure S4B), and >90% of nanoparticles exhibited D_{eff} greater than 0.1 $\mu m^2/s$ (Figure S4C). The average speeds of $PLGA_{5.6k}$/$PLGA_{20k}$–PEG_{5k}, $PLGA_{18k}$/$PLGA_{20k}$–PEG_{5k}, $PLGA_{55k}$/$PLGA_{20k}$–PEG_{5k} (polymers blended 1:1 by weight) and $PLGA_{45k}$–PEG_{5k} nanoparticles were similar, and only 6-, 5-, 5-, and 7-fold lower than the theoretical diffusion rates of similarly sized nanoparticles in water, respectively (Table 2).

Although the PEG surface density was similar for these four formulations, the drug loading and release properties varied. $PLGA_{45k}$–PEG_{5k} nanoparticles, prepared from the diblock copolymer without blending, provided the lowest encapsulation efficiency (EE) of 24% and drug loading (DL) of 2.2% for PTX. In contrast, the blended nanoparticles resulted in significantly higher EE and DL. The blending of $PLGA_{5.6k}$ and $PLGA_{20k}$–PEG_{5k} 1:1 by weight provided 76% EE and 6.9% DL (Table 2). Increased drug loading allows for the same amount of drug to be delivered with less polymer. In addition to the decreased PTX loading observed with the $PLGA_{45k}$–PEG_{5k} nanoparticles, the drug release was also more rapid. The time for 50% of loaded drug to be released ($T_{1/2}$) from $PLGA_{45k}$–PEG_{5k} nanoparticles was only about 1.5 days. In comparison, the blended nanoparticles provided more sustained release, with $PLGA_{45k}$/$PLGA_{20k}$-PEG_{5k} nanoparticles having a $T_{1/2}$ of approximately 6 days (Figure S5). Therefore, it is clear that the overall PEG content, the molecular weight of the PEG, and the molecular weight of the PLGA polymer all affect the drug release properties.[37]

Formulation methods that allow for specific tuning of the drug loading and release properties, while also maintaining surface properties for effective mucosal delivery, provide a platform for designing drug delivery strategies for a wide variety of therapeutic applications and target sites. Furthermore, nanoparticle formulations with high surface PEG density and high drug loading also have potential for improved systemic drug delivery. Dense PEG coatings on nanoparticle surfaces can provide increased blood circulation time,[38−40] leading to increased accumulation in tumors *via* the enhanced permeation and retention (EPR) effect,[41] targeting of other diseases characterized by abnormal neovascularization (several ocular disorders, diabetes, obesity, asthma, multiple sclerosis, *etc.*),[42] and improved delivery across the blood brain barrier following the application of focused ultrasound (FUS),[43] among others. It has been found that anti-PEG IgM antibodies can be generated after the intravenous injection of PEGylated liposomes,[44−46] and the anti-PEG antibodies were regarded as the main serum factor responsible for accelerated blood clearance (ABC) of the systemically administered nanoparticles.[44] However, it is not known

whether there is an endogenous presence of anti-PEG antibodies in mucus secretions, or whether antibodies are generated in response to mucosal exposure to PEGylated nanoparticles. It has been demonstrated that multivalent interactions with exogenous anti-HSV (herpes simplex virus) IgG added to neutralized human cervicovaginal mucus (0.333−1 μg/mL) can trap HSV, and reduced rates of vaginal HSV infection in a mouse model.[47] However, it is unlikely that dosing PEG-coated nanoparticles at mucosal surfaces would lead to the generation of anti-PEG antibodies at levels sufficient to trap PEGylated nanoparticles in mucus. Further work in this area will be important in the development of the MPP technology.

CONCLUSION

We have developed a method for formulating biodegradable nanoparticles with varying PEG surface density. As PEG surface density increased, the binding of mucin to nanoparticle surfaces *in vitro* decreased, and the nanoparticle transport rates in human CVM *ex vivo* increased. Increasing PEG surface density increases steric hindrance experienced by the PEG chains, likely resulting in a conformational change in the surface PEG molecules from mushroom to brush to dense brush. For these PLGA−PEG blend formulations, rapid diffusion in human CVM and improved vaginal distribution in mice *in vivo* was achieved with a dense brush conformation. The exact PEG surface density necessary for mucus penetration may vary depending on the core materials used, nanoparticle size, PEG molecular weight, and the type of mucus studied.

Uniform coverage of the vaginal surface by nanoparticles with high PEG surface density indicates that these formulations may be effective for various vaginal drug delivery applications, including prevention of sexually transmitted infections.[10] These formulations can also be adjusted for loading various drugs for a variety of mucosal diseases, including cancer, inflammation, and infections at a variety of mucosal surfaces, including the eyes, gastrointestinal tract, and respiratory tract. Furthermore, we were able to modify the drug loading and drug release profiles through polymer blending, providing methodology for further tuning nanoparticle design for various mucosal applications.

MATERIALS AND METHODS

Materials. Poly(lactic-*co*-glycolic acid) polymers (PLGA; LA/GA molar ratio 50:50; acid end group) with inherent viscosities of 0.05−0.15 dL/g (PLGA1A, Mw ~5.6 kDa and PDI ~2.5), 0.15−0.25 dL/g (PLGA2A, Mw ~18 kDa and PDI ~3.1) and 0.35−0.45 dL/g (PLGA4A, Mw ~55 kDa and PDI ~1.7), respectively, were purchased from Lakeshore Biomaterials (Evonik Corporation, Birmingham, AL). The molecular weights of the three polymers were provided by the supplier. The block copolymers of PLGA(LA/GA 50:50) and monomethoxy poly(ethylene glycol), $PLGA_{45k}$−PEG_{5k} and $PLGA_{15k}$−PEG_{5k}, were custom-synthesized by the Daigang Biomaterial Co., Ltd., (Jinan, China) and characterized by ^{1}H NMR and GPC. A Waters GPC system equipped with a refractive index detector and two Waters Styragel columns (HR3 and HR4) were used. The analysis was performed at 30 °C using chloroform as the mobile phase and a flow rate of 0.3 mL/min. The GPC was calibrated with polystyrene standards (Walters) of known MW. Cholic acid sodium salt (CHA), polyethylene glycol (Mw 5 kDa), and mucin from bovine submaxillary glands (type I−S) were purchased from Sigma-Aldrich (St. Louis, MO). Alexa Fluor 555 cadaverine (AF555) was purchased from Invitrogen (Eugene, OR).

Preparation and Characterization of Nanoparticles. Nanoparticles were prepared by the emulsification method using 0.5 (w/vol %) CHA solution, as reported previously.[11] In brief, PLGA and PLGA−PEG at determined ratios (total 50 mg) were dissolved in dichloromethane, and the oil phase was poured into 5 mL of 0.5% sodium cholate solution under probe sonication (30% amplitude) for 2 min. The emulsion was added to another 35 mL of 0.5% CHA solution under magnetic stirring (700 rpm) to evaporate the organic solvent. Nanoparticles were filtered through 1 μm membrane filters, collected by centrifugation at 20 000*g* for 25 min, and thoroughly washed with water. To prepare nanoparticles for fluorescence microscopy, Alexa Fluor 555-labeled polymers[11] (~25% by weight) were blended with unlabeled polymers prior to emulsification.

Nanoparticles were prepared by nanoprecipitation as follows. $PLGA_{45k}$−PEG_{5k} was dissolved in acetonitrile at a concentration of 25 mg/mL and dispensed using a syringe into DI water under magnetic stirring (700 rpm). After the complete removal of organic solvent by evaporation, nanoparticles were collected as described above.

The diameter, polydispersity index (PDI), and surface charge (ζ-potential) of nanoparticles were determined by dynamic light scattering and laser Doppler anemometry using a Zetasizer Nano ZS90 (Malvern Instruments, Southborough, MA). Measurements were performed with nanoparticles dispersed in 10 mM NaCl solution (pH 7). The morphology of nanoparticles was characterized by transmission electron microscopy (TEM) on H7600 TEM (Hitachi, Japan).

Drug Encapsulation and Release Studies. To encapsulate drug, 5 mg of PTX was mixed with 50 mg of polymer ($PLGA_{45k}$−PEG_{5k} and blends of $PLGA_{(5.6k,18k,55k)}$/$PLGA_{20k}$−PEG_{5k} at 1:1 ratio). The emulsification method was used as described above. A known amount of PTX-loaded nanoparticles was freeze-dried, weighed, and dissolved in acetonitrile for HPLC measurement. The drug loading (DL) and encapsulation efficiency (EE) were calculated according to the following equations:

$$\text{DL}\ (\%) = (\text{amount of PTX in nanoparticles}/\text{weight of nanoparticles}) \times 100\%$$

$$\text{EE}\ (\%) = (\text{drug loading measured}/\text{theoretical drug loading}) \times 100\%$$

Drug release was conducted by suspending nanoparticles in 1 mL PBS containing 0.2 (v/vol %) Tween 20 sealed in a dialysis tubing cellulose membrane (MW cutoff: 100 kDa). The sealed dialysis membrane was placed into a 50 mL conical tube containing 20 mL of release media (PBS containing 0.2 (v/vol %) Tween 20) and incubated at 37 °C on a platform shaker (140 rpm). The entire volume of release media was collected at predetermined intervals and replaced with another 20 mL of fresh release media. The PTX concentration in the collected release media was measured by HPLC. Isocratic separation was performed on a Shimadzu Prominence LC system (Kyoto, Japan) equipped with a Pursuit 5 C18 column (Varian, Inc., Lake Forest, CA) and mobile phase consisting of acetonitrile/water (65/35 (v/v)) containing 0.1% trifluoroacetic acid (flow rate = 1 mL/min). Column effluent was monitored by UV detection at 230 nm.

Quantification of Surface PEG Density. The surface PEG density on nanoparticles was determined by ^{1}H NMR using Bruker 400 REM instrument at 400 mHz.[11,48,49] Relaxation time was set at 10 s, and ZG at 90°. Nanoparticles with various PEG contents were directly prepared in 0.5% CHA D_2O solution and suspended in D_2O with 1 wt % 3-(trimethylsilyl)-1-propanesulfonic acid, sodium salt (DSS) as an internal standard for ^{1}H NMR analysis. A known mass of PEG_{5k} (Sigma, St Louis, MO) homopolymer in D_2O with 1% DSS was serially diluted for generation of a calibration curve for the PEG signal in ^{1}H NMR, and this calibration curve was used to calculate the surface PEG content on nanoparticles. To determine the mass fraction of nanoparticles in solution, 0.2 mL of nanoparticle D_2O solution was lyophilized and weighed. The surface PEG density was calculated as the number of PEG molecules per 100 nm^2 surface area on nanoparticles, assuming all surface PEG chains were full length. Control ^{1}H NMR experiments were also performed on CHA D_2O solution and PLGA nanoparticles prepared by the same method, and there were no detectable CHA peaks in the spectrum of the PLGA nanoparticles.

The PEG density, [Γ], representing the number of PEG molecules on the nanoparticle surface per 100 nm^2 was calculated by dividing the total PEG content (M_{PEG}, in mole) detected by ^{1}H NMR by the total surface area of all nanoparticles.

$$[\Gamma] = \frac{M_{PEG} \times 6.02 \times 10^{23}}{W_{NP}/d_{NP}/\frac{4}{3}\pi\left(\frac{D}{2}\right)^3}/4\pi\left(\frac{D}{2}\right)^2$$

Where W_{NP} is the total mass of nanoparticles, d_{NP} is the density of nanoparticle (here we assuming the density of nanoparticles was equal to the density of polymer, 1.22 g/mL for PLGA), and D is the diameter of nanoparticles as measured by dynamic light scattering.

According to the report by Auguste and co-workers,[50] full surface mushroom coverage [Γ*] represents the number of unconstrained PEG molecules per 100 nm^2. To determine [Γ*], the surface area occupied by one PEG chain was estimated assuming random-walk statistics and that the PEG chain occupies an area at the interface given by a sphere of diameter ξ.

$$\xi = 0.76m^{0.5}\ [\text{Å}]$$

where m is the molecular weight of PEG chain. The surface area occupied by one PEG molecule can be determined from $(\xi/2)^2$. Thus, PEG_{5k} has an unconstrained molecule sphere with diameter of 5.4 nm, and occupies a surface area of 22.7 nm^2. Thus, the number of PEG molecules to fully cover 100 nm^2 surface area, [Γ*], is 4.4. The ratio [Γ]/[Γ*] to reflects how densely the PEG is packed on the nanoparticle surface: a ratio <1 indicates low density and PEG molecules are in mushroom conformation; >2 indicates high density and the PEG molecules are in a dense brush conformation.

Quantification of Total PEG Content in Nanoparticles. The total nanoparticle PEG content was determined by ^{1}H NMR using Bruker 400 REM instrument at 400 mHz. The lyophilized nanoparticles were weighed and dissolved in $CDCl_3$ containing 1 wt % hexadeuterodimethyl sulfoxide (TMS) as an internal standard. The PEG content was determined by comparing to a PEG_{5k} calibration curve calculated from ^{1}H NMR spectra using TMS as internal standard.

Multiple Particle Tracking. The tracking of fluorescently labeled nanoparticles in fresh human cervicovaginal mucus (CVM) was performed as previously described.[51,52] Each nanoparticle formulation was tested in CVM samples from 3 self-reported healthy individuals with no vaginal symptoms. Briefly, 0.6 μL of nanoparticles at 500 times dilution was mixed into 20 μL of mucus (~3% v/v), sealed with a coverslip, and incubated for 1 h prior to microscopy. Movies were captured at a temporal resolution of 66.7 ms for 20 s using a silicon-intensified target camera (VE-1000, Dage-MTI) mounted on an inverted epifluorescence microscope equipped with a 100× oil-immersion objective lens. Trajectories for $n > 120$ particles per experiment were extracted using MetaMorph software (Universal Imaging). Time averaged mean square displacement (MSD) and effective diffusivity (D_{eff}) values were calculated for each particle as a function of time scale. A one-tailed, unequal variance Student's t-test was used to evaluate significance ($P < 0.05$).

Nanoparticle Stability *in Vitro*. Nanoparticles (~10 mg/mL) with different target PEG contents (0%, 2%, 3%, 5%, 8%, 10%, and 25% PEG) were incubated with 10 mg/mL mucin (from bovine submaxillary gland; Sigma, St. Louis, MO) solution at 37 °C under gentle stirring. The stock mucin solution was prepared by dissolving the mucin solids into distilled water followed by centrifugation at 10 000g for 30 min to remove undissolved solids. The final mucin concentration was determined by carefully weighing a portion of lyophilized mucin solution. At each time point, an aliquot of nanoparticle solution was collected to measure nanoparticle size using the dynamic light scattering on Zetasizer Nano ZS90. The measurements were performed in triplicate at room temperature.

Mucin Binding Assay Using Isothermal Titration Calorimetry. The stoichiometry of mucin binding to nanoparticles with different PEG surface densities was determined by Isothermal Titration Calorimetry using a VP-ITC from MicroCal/GE Healthcare (Northampton, MA). The titrations were performed at 25 °C by injecting 10 μL aliquots of mucin solution into the calorimetric cell (volume ~1.4 mL) containing the suspension of nanoparticles. The concentration of nanoparticles was 1 mg/mL for nanoparticles with target PEG contents of 0−8% and 1.5 mg/mL for nanoparticles with target PEG contents of 10 and 25%. The concentrations of mucin were 2.22 and 1.11 mg/mL for the titrations of nanoparticles with target PEG contents of 0−3% and 5−25%, respectively. Both reagents were prepared directly in water. The heat evolved upon each injection of inhibitor was obtained from the integral of the calorimetric signal. The heat associated with the binding reaction was obtained by subtracting the heat of dilution from the heat of reaction. The individual heats were plotted against the molar ratio, and the stoichiometry was obtained by nonlinear regression of the data. Stoichiometry was applied to calculate the amount of mucin bound to the nanoparticle surface (presented as mg mucin per m^2).

Distribution of Nanoparticles in Mouse Vagina. To investigate the effect of PEG surface density on nanoparticle distribution in the mouse vagina, we used 6−8 week old female CF-1 mice (Harlan Laboratories). Mice were housed in a reversed light cycle facility (12-h light/12-h dark) and selected for estrus appearance, as described previously.[10] Mice were anesthetized before experimental procedures. All experimental protocols were approved by the Johns Hopkins Animal Care and Use Committee.

The distribution of nanoparticles with different target PEG contents (0%, 3%, 10% and 25% PEG) in the mouse vagina was assessed as described previously.[10] Briefly, 5 μL of nanoparticles was administered intravaginally. Within 10 min, the entire vagina was then removed and frozen in Tissue-Tek OCT Compound (Sakura Finetek U.S.A. Inc.). Transverse sections were obtained at various points along the length of the tissue (between the introitus and the cervix) with a Microm HM 500 M Cryostat (Microm International). The thickness of the sections was set to 6 μm to achieve single-cell layer thickness. The sections were then stained with ProLongGold (Invitrogen) antifade reagent with 4,6-diamidino-2-phenylindole (DAPI) to visualize cell nuclei and retain particle fluorescence. Images of the sections were obtained with an inverted fluorescence microscope. To quantify nanoparticle distribution, vaginal tissues were sliced open longitudinally and clamped between two glass slides sealed with superglue. This procedure flattens the tissue, exposing the folds ("rugae"). A blank tissue was used to assess background tissue fluorescence levels to ensure that all images taken were well above background levels. Six fluorescence images at low magnification and at least one image at high magnification were taken for each tissue. The images were thresholded to draw boundaries around the fluorescence signal, and then the area covered was quantified with ImageJ software. An average coverage was determined for each mouse, and then these values were averaged over a group of $n \geq 3$ mice. *$p < 0.05$, **$p < 0.01$ and ***$p < 0.001$ (one-tailed, unequal variance Student's t-test).

Conflict of Interest: The authors declare the following competing financial interest(s): The mucus-penetrating particle technology described in this publication is being developed by

Kala Pharmaceuticals. Dr. Hanes is co-founder of Kala and serves on its Board of Directors. Dr. Hanes owns company stock, which is subject to certain restrictions under Johns Hopkins University policy. The terms of this arrangement are being managed by Johns Hopkins University in accordance with its conflict of interest policies.

Acknowledgment. We thank the Wilmer Microscopy and Imaging Core and the Drug Delivery and Nanotechnology Core of the Wilmer Eye Institute, each of which are supported by the NIH (P30-EY001765). This work was supported in part by the NIH R33AI07974 (J.H.), NIH R01HD062844 (J.H.), NIH GM056550 (A.S. and E.F.) and NSF MCB-1157506 (A.S. and E.F.). We also acknowledge the Raymond Kwok Family Research Fund, USA (J.H. and Q.X.), the Johns Hopkins University Center for AIDS Research P30AI094189 (L.M.E.), the W.W. Smith Charitable Trust A1302 (L.M.E.) and the China Scholarship Council (X.G.).

Supporting Information Available: The Supporting Information is available free of charge on the ACS Publications website at DOI: 10.1021/acsnano.5b03876.

Additional experimental details (PDF)

REFERENCES AND NOTES

1. Patel, V. F.; Liu, F.; Brown, M. B. Advances in Oral Transmucosal Drug Delivery. *J. Controlled Release* **2011**, *153*, 106–116.
2. Torres-Lugo, M.; Peppas, N. A. Transmucosal Delivery Systems for Calcitonin: a Review. *Biomaterials* **2000**, *21*, 1191–1196.
3. Ensign, L. M.; Schneider, C.; Suk, J. S.; Cone, R.; Hanes, J. Mucus Penetrating Nanoparticles: Biophysical Tool and Method of Drug and Gene Delivery. *Adv. Mater.* **2012**, *24*, 3887–3894.
4. Rosen, H.; Abribat, T. The Rise and Rise of Drug Delivery. *Nat. Rev. Drug Discovery* **2005**, *4*, 381–385.
5. LaVan, D. A.; McGuire, T.; Langer, R. Small-scale Systems for *In Vivo* Drug Delivery. *Nat. Biotechnol.* **2003**, *21*, 1184–1191.
6. Cone, R. A. Barrier Properties of Mucus. *Adv. Drug Delivery Rev.* **2009**, *61*, 75–85.
7. Lai, S. K.; Wang, Y.-Y.; Hanes, J. Mucus-penetrating Nanoparticles for Drug and Gene Delivery to Mucosal Tissues. *Adv. Drug Delivery Rev.* **2009**, *61*, 158–171.
8. Wang, Y. Y.; Lai, S. K.; Suk, J. S.; Pace, A.; Cone, R.; Hanes, J. Addressing the PEG Mucoadhesivity Paradox to Engineer Nanoparticles that "Slip" through the Human Mucus Barrier. *Angew. Chem., Int. Ed.* **2008**, *47*, 9726–9729.
9. Yang, M.; Lai, S. K.; Wang, Y. Y.; Zhong, W. X.; Happe, C.; Zhang, M.; Fu, J.; Hanes, J. Biodegradable Nanoparticles Composed Entirely of Safe Materials that Rapidly Penetrate Human Mucus. *Angew. Chem., Int. Ed.* **2011**, *50*, 2597–2600.
10. Ensign, L. M.; Tang, B. C.; Wang, Y.-Y.; Tse, T. A.; Hoen, T.; Cone, R.; Hanes, J. Mucus-penetrating Nanoparticles for Vaginal Drug Delivery Protect against Herpes Simplex Virus. *Sci. Transl. Med.* **2012**, *4*, 138ra79.
11. Xu, Q.; Boylan, N. J.; Cai, S.; Miao, B.; Patel, H.; Hanes, J. Scalable Method to Produce Biodegradable Nanoparticles that Rapidly Penetrate Human Mucus. *J. Controlled Release* **2013**, *170*, 279–286.
12. Walkey, C. D.; Olsen, J. B.; Guo, H.; Emili, A.; Chan, W. C. W. Nanoparticle Size and Surface Chemistry Determine Serum Protein Adsorption and Macrophage Uptake. *J. Am. Chem. Soc.* **2012**, *134*, 2139–2147.
13. Perry, J. L.; Reuter, K. G.; Kai, M. P.; Herlihy, K. P.; Jones, S. W.; Luft, J. C.; Napier, M.; Bear, J. E.; DeSimone, J. M. PEGylated PRINT Nanoparticles: The Impact of PEG Density on Protein Binding, Macrophage Association, Biodistribution, and Pharmacokinetics. *Nano Lett.* **2012**, *12*, 5304–5310.
14. Hak, S.; Helgesen, E.; Hektoen, H. H.; Huuse, E. M.; Jarzyna, P. A.; Mulder, W. J. M.; Haraldseth, O.; Davies, C. d. L. The Effect of Nanoparticle Polyethylene Glycol Surface Density on Ligand-Directed Tumor Targeting Studied *in Vivo* by Dual Modality Imaging. *ACS Nano* **2012**, *6*, 5648–5658.
15. Beletsi, A.; Panagi, Z.; Avgoustakis, K. Biodistribution Properties of Nanoparticles Based on Mixtures of PLGA with PLGA–PEG Diblock Copolymers. *Int. J. Pharm.* **2005**, *298*, 233–241.
16. Mosqueira, V. C. F.; Legrand, P.; Morgat, J. L.; Vert, M.; Mysiakine, E.; Gref, R.; Devissaguet, J. P.; Barratt, G. Biodistribution of Long-Circulating PEG-grafted Nanocapsules in Mice: Effects of PEG Chain Length and Density. *Pharm. Res.* **2001**, *18*, 1411–1419.
17. Cu, Y.; Saltzman, W. M. Controlled Surface Modification with Poly(Ethylene Glycol) Enhances Diffusion of PLGA Nanoparticles in Human Cervical Mucus. *Mol. Pharmaceutics* **2009**, *6*, 173–181.
18. Nance, E. A.; Woodworth, G. F.; Sailor, K. A.; Shih, T.-Y.; Xu, Q.; Swaminathan, G.; Xiang, D.; Eberhart, C.; Hanes, J. A Dense Poly(Ethylene Glycol) Coating Improves Penetration of Large Polymeric Nanoparticles within Brain Tissue. *Sci. Transl. Med.* **2012**, *4*, 149ra119.
19. Vila, A.; Gill, H.; McCallion, O.; Alonso, M. J. Transport of PLA-PEG Particles across the Nasal Mucosa: Effect of Particle Size and PEG Coating Density. *J. Controlled Release* **2004**, *98*, 231–244.
20. Pino, P. d.; Pelaz, B.; Zhang, Q.; Maffre, P.; Nienhaus, G. U.; Parak, W. J. Protein Corona Formation around Nanoparticles - From the Past to the Future. *Mater. Horiz.* **2014**, *1*, 301–313.
21. Pelaz, B.; del Pino, P.; Maffre, P.; Hartmann, R.; Gallego, M.; Rivera-Fernández, S.; de la Fuente, J. M.; Nienhaus, G. U.; Parak, W. J. Surface Functionalization of Nanoparticles with Polyethylene Glycol: Effects on Protein Adsorption and Cellular Uptake. *ACS Nano* **2015**, *9*, 6996–7008.
22. Zhang, L.; Chan, J. M.; Gu, F. X.; Rhee, J.-W.; Wang, A. Z.; Radovic-Moreno, A. F.; Alexis, F.; Langer, R.; Farokhzad, O. C. Self-Assembled Lipid–Polymer Hybrid Nanoparticles: A Robust Drug Delivery Platform. *ACS Nano* **2008**, *2*, 1696–1702.
23. Lai, S. K.; O'Hanlon, D. E.; Harrold, S.; Man, S. T.; Wang, Y. Y.; Cone, R.; Hanes, J. Rapid Transport of Large Polymeric Nanoparticles in Fresh Undiluted Human Mucus. *Proc. Natl. Acad. Sci. U. S. A.* **2007**, *104*, 1482–1487.
24. Lai, S. K.; Suk, J. S.; Pace, A.; Wang, Y.-Y.; Yang, M.; Mert, O.; Chen, J.; Kim, J.; Hanes, J. Drug Carrier Nanoparticles that Penetrate Human Chronic Rhinosinusitis Mucus. *Biomaterials* **2011**, *32*, 6285–6290.
25. Suk, J. S.; Lai, S. K.; Wang, Y. Y.; Ensign, L. M.; Zeitlin, P. L.; Boyle, M. P.; Hanes, J. The Penetration of Fresh Undiluted Sputum Expectorated by Cystic Fibrosis Patients by Non-adhesive Polymer Nanoparticles. *Biomaterials* **2009**, *30*, 2591–2597.
26. Lindman, S.; Lynch, I.; Thulin, E.; Nilsson, H.; Dawson, K. A.; Linse, S. Systematic Investigation of the Thermodynamics of HSA Adsorption to N-iso-Propylacrylamide/N-tert-Butylacrylamide Copolymer Nanoparticles. Effects of Particle Size and Hydrophobicity. *Nano Lett.* **2007**, *7*, 914–920.
27. Monopoli, M. P.; Walczyk, D.; Campbell, A.; Elia, G.; Lynch, I.; Baldelli Bombelli, F.; Dawson, K. A. Physical-Chemical Aspects of Protein Corona: Relevance to *In Vitro* and *In Vivo* Biological Impacts of Nanoparticles. *J. Am. Chem. Soc.* **2011**, *133*, 2525–2534.
28. Liedl, T.; Keller, S.; Simmel, F. C.; Rädler, J. O.; Parak, W. J. Fluorescent Nanocrystals as Colloidal Probes in Complex Fluids Measured by Fluorescence Correlation Spectroscopy. *Small* **2005**, *1*, 997–1003.
29. Gref, R.; Lück, M.; Quellec, P.; Marchand, M.; Dellacherie, E.; Harnisch, S.; Blunk, T.; Müller, R. H. 'Stealth' Corona-Core Nanoparticles Surface Modified by Polyethylene Glycol (PEG): Influences of the Corona (PEG Chain Length and Surface Density) and of the Core Composition on Phagocytic Uptake and Plasma Protein Adsorption. *Colloids Surf., B* **2000**, *18*, 301–313.
30. Dos Santos, N.; Allen, C.; Doppen, A.-M.; Anantha, M.; Cox, K. A. K.; Gallagher, R. C.; Karlsson, G.; Edwards, K.; Kenner, G.; Samuels, L.; et al. Influence of Poly(Ethylene Glycol) Grafting Density and Polymer Length on Liposomes: Relating Plasma Circulation Lifetimes to Protein Binding. *Biochim. Biophys. Acta, Biomembr.* **2007**, *1768*, 1367–1377.

31. Omar, R. F.; Trottier, S.; Brousseau, G.; Lamarre, A.; Alexandre, G.; Bergeron, M. G. Distribution of a Vaginal Gel (Invisible Condom®) before, during and after Simulated Sexual Intercourse and its Persistence when Delivered by Two Different Vaginal Applicators: A Magnetic Resonance Imaging Study. *Contraception* **2008**, *77*, 447–455.
32. Mauck, C. K.; Katz, D.; Sandefer, E. P.; Nasution, M. D.; Henderson, M.; Digenis, G. A.; Su, I.; Page, R.; Barnhart, K. Vaginal Distribution of Replens® and K-Y® Jelly Using Three Imaging Techniques. *Contraception* **2008**, *77*, 195–204.
33. Barnhart, K. T.; Pretorius, E. S.; Shaunik, A.; Timbers, K.; Nasution, M.; Mauck, C. Vaginal Distribution of Two Volumes of the Novel Microbicide Gel Cellulose Sulfate (2.5 and 3.5 mL). *Contraception* **2005**, *72*, 65–70.
34. Achilles, S. L.; Shete, P. B.; Whaley, K. J.; Moench, T. R.; Cone, R. A. Microbicide Efficacy and Toxicity Tests in a Mouse Model for Vaginal Transmission of Chlamydia trachomatis. *Sex. Transm. Dis.* **2002**, *29*, 655–664.
35. Ensign, L. M.; Hoen, T. E.; Maisel, K.; Cone, R. A.; Hanes, J. S. Enhanced Vaginal Drug Delivery through the Use of Hypotonic Formulations that Induce Fluid Uptake. *Biomaterials* **2013**, *34*, 6922–6929.
36. Yang, M.; Yu, T.; Wang, A. Z.; Lai, S. K.; Zeng, Q.; Miao, B.; Tang, B. C.; Simons, B. W.; Ensign, L.; Liu, G.; et al. Vaginal Delivery of Paclitaxel *via* Nanoparticles with Non-Mucoadhesive Surfaces Suppresses Cervical Tumor Growth. *Adv. Healthcare Mater.* **2014**, *3*, 1044–1052.
37. Matsumoto, J.; Nakada, Y.; Sakurai, K.; Nakamura, T.; Takahashi, Y. Preparation of Nanoparticles Consisted of Poly(L-Lactide)-Poly(Ethylene Glycol)-Poly(L-Lactide) and Their Evaluation *In Vitro*. *Int. J. Pharm.* **1999**, *185*, 93–101.
38. Owens, D. E.; Peppas, N. A. Opsonization, Biodistribution, and Pharmacokinetics of Polymeric Nanoparticles. *Int. J. Pharm.* **2006**, *307*, 93–102.
39. Gref, R.; Minamitake, Y.; Peracchia, M. T.; Trubetskoy, V.; Torchilin, V.; Langer, R. Biodegradable Long-Circulating Polymeric Nanospheres. *Science* **1994**, *263*, 1600–1603.
40. Gref, R.; Domb, A.; Quellec, P.; Blunk, T.; Muller, R. H.; Verbavatz, J. M.; Langer, R. The Controlled Intravenous Delivery of Drugs Using PEG-Coated Sterically Stabilized Nanospheres. *Adv. Drug Delivery Rev.* **1995**, *16*, 215–233.
41. Fang, J.; Nakamura, H.; Maeda, H. The EPR Effect: Unique Features of Tumor Blood Vessels for Drug Delivery, Factors Involved, and Limitations and Augmentation of the Effect. *Adv. Drug Delivery Rev.* **2011**, *63*, 136–151.
42. Alexis, F.; Pridgen, E.; Molnar, L. K.; Farokhzad, O. C. Factors Affecting the Clearance and Biodistribution of Polymeric Nanoparticles. *Mol. Pharmaceutics* **2008**, *5*, 505–515.
43. Nance, E.; Timbie, K.; Miller, G. W.; Song, J.; Louttit, C.; Klibanov, A. L.; Shih, T.-Y.; Swaminathan, G.; Tamargo, R. J.; Woodworth, G. F.; et al. Non-Invasive Delivery of Stealth, Brain-Penetrating Nanoparticles across the Blood-Brain Barrier Using MRI-Guided Focused Ultrasound. *J. Controlled Release* **2014**, *189*, 123–132.
44. Ishida, T.; Ichihara, M.; Wang, X.; Yamamoto, K.; Kimura, J.; Majima, E.; Kiwada, H. Injection of PEGylated Liposomes in Rats Elicits PEG-Specific IgM, which is Responsible for Rapid Elimination of a Second Dose of PEGylated Liposomes. *J. Controlled Release* **2006**, *112*, 15–25.
45. Ichihara, M.; Shimizu, T.; Imoto, A.; Hashiguchi, Y.; Uehara, Y.; Ishida, T.; Kiwada, H. Anti-PEG IgM Response Against PEGylated Liposomes in Mice and Rats. *Pharmaceutics* **2010**, *3*, 1.
46. Ishida, T.; Harada, M.; Wang, X. Y.; Ichihara, M.; Irimura, K.; Kiwada, H. Accelerated Blood Clearance of PEGylated Liposomes Following Preceding Liposome Injection: Effects of Lipid Dose and PEG Surface-Density and Chain Length of the First-Dose Liposomes. *J. Controlled Release* **2005**, *105*, 305–317.
47. Wang, Y. Y.; Kannan, A.; Nunn, K. L.; Murphy, M. A.; Subramani, D. B.; Moench, T.; Cone, R.; Lai, S. K. IgG in Cervicovaginal Mucus Traps HSV and Prevents Vaginal Herpes Infections. *Mucosal Immunol.* **2014**, *7*, 1036–1044.
48. Heald, C. R.; Stolnik, S.; Kujawinski, K. S.; De Matteis, C.; Garnett, M. C.; Illum, L.; Davis, S. S.; Purkiss, S. C.; Barlow, R. J.; Gellert, P. R. Poly(Lactic Acid)-Poly(Ethylene Oxide) (PLA-PEG) Nanoparticles: NMR Studies of the Central Solidlike PLA Core and the Liquid PEG Corona. *Langmuir* **2002**, *18*, 3669–3675.
49. Garcia-Fuentes, M.; Torres, D.; Martin-Pastor, M.; Alonso, M. J. Application of NMR Spectroscopy to the Characterization of PEG-Stabilized Lipid Nanoparticles. *Langmuir* **2004**, *20*, 8839–8845.
50. Auguste, D. T.; Armes, S. P.; Brzezinska, K. R.; Deming, T. J.; Kohn, J.; Prud'homme, R. K. pH Triggered Release of Protective Poly(Ethylene Glycol)-*b*-Polycation Copolymers from Liposomes. *Biomaterials* **2006**, *27*, 2599–2608.
51. Lai, S. K.; Wang, Y. Y.; Hida, K.; Cone, R.; Hanes, J. Nanoparticles Reveal that Human Cervicovaginal Mucus is Riddled with Pores Larger than Viruses. *Proc. Natl. Acad. Sci. U. S. A.* **2010**, *107*, 598–603.
52. Tang, B. C.; Dawson, M.; Lai, S. K.; Wang, Y.-Y.; Suk, J. S.; Yang, M.; Zeitlin, P.; Boyle, M. P.; Fu, J.; Hanes, J. Biodegradable Polymer Nanoparticles that Rapidly Penetrate the Human Mucus Barrier. *Proc. Natl. Acad. Sci. U. S. A.* **2009**, *106*, 19268–19273.